Article:
Laib, A., Chelabi, M., Terriche, Y. et al. (4 more authors) (2024) Enhanced complex wire fault diagnosis via integration of time domain reflectometry and particle swarm optimization with least square support vector machine. IET Science, Measurement & Technology, 18 (8). pp. 417-428. ISSN 1751-8822

https://doi.org/10.1049/smt2.12187

Received: 16 August 2023 | Revised: 29 January 2024 | Accepted: 26 February 2024

IET Science, Measurement & Technology

DOI: 10.1049/smt2.12187

The Institution of Engineering and Technology WILEY

ORIGINAL RESEARCH

Enhanced complex wire fault diagnosis via integration of time domain reflectometry and particle swarm optimization with least square support vector machine

Abderrzak Laib[1] | **Mohamed Chelabi**[2] | **Yacine Terriche**[3] | **Mohammed Melit**[2] | **Hamza Boudjefdjouf**[4] | **Hafiz Ahmed**[5] | **Zakaria Chedjara**[6]

[1]Department of Electrical Engineering Faculty of technology, University of M'sila, M'sila, Algeria

[2]Department of Electrical Engineering, Jijel University, Jijel, Algeria

[3]Ørsted Wind Power A/S, Fredericia, Denmark

[4]Department of Electrical Engineering, University of Freres Mentouri Constantine, Constantine, Algeria

[5]Nuclear AMRC, The University of Sheffield, Derby, UK

[6]Faculty of Applied Sciences, Ibn Khaldoun University of Tiaret Algeria, Tiaret, Algeria

Correspondence
Hafiz Ahmed, Nuclear AMRC Midlands, The University of Sheffield, Rutherford Way, Infinity Pk Wy, Derby, DE73 5SS, UK.
Email: hafiz.ahmed@sheffield.ac.uk, hafiz.h.ahmed@ieee.org

Abstract

Urban power systems rely on intricate wire networks, known as the power grid, which form the essential electric infrastructure in cities. While these networks transmit electricity from power plants to consumers, they are vulnerable to faults caused by manufacturing errors and improper installation, posing risks to system integrity. Thus, accurate identification and assessment of these faults are crucial to prevent damage and maintain system reliability. The objective of this research is to present an innovative and efficient methodology for diagnosing complex wire networks through the application of time domain reflectometry (TDR) combined with the particle swarm optimization (PSO) and least squares support vector machine (LSSVM) algorithm. This research addresses the imperative need to accurately locate and assess breakage faults within wire networks, emphasizing their role in both power transmission and communication infrastructure. To model the TDR answer of a specific complex wire network, a forward model is established utilizing resistance, inductance, capacitance and conductance (RLCG) parameters and the finite difference time domain (FDTD) method. Subsequently, the PSO-LSSVM approach is used to solve the inverse problem of localizing faults in complex wire networks. The experimental results validate the practicality of this approach in real-world systems.

1 | INTRODUCTION

Ensuring safety is paramount for the dependable operation of modern systems reliant on electric wire networks. These networks work as the main method of transporting energy and information in an extensive range of applications, including transportation, industrial machinery, power distribution, and building systems. Various types of cables are used for different purposes, with their applications varying depending on factors, such as the type of signal being transmitted, voltage levels, and environmental conditions. Cables selected for energy networks differ from those used in data networks due to their particular design, specifically tailored for efficient power distribution. This work focuses on the diagnostic assessment of complex wire networks, which are vital components of the power grid serving both power and communication purposes. Coaxial cables, characterized by a central conductor, insulating layer, and metallic shield, excel in diverse transmission line applications such as data transfer, telecommunications, and cable television (TV). With their capacity for high-frequency transmission over extended distances, broad frequency support, and effective shielding against interference, coaxial cables play a pivotal role in ensuring dependable signal integrity. From television distribution and internet connectivity to closed-circuit TV (CCTV) systems, their versatile applications underscore their significance in maintaining stable and interference-free signal transmission across various industries. Coaxial cables can experience various degradation mechanisms, such as chemical, electrical, mechanical, or aging processes, resulting in faults and failures within different systems. There are two categories in

which these faults appear: when confronted with simple and limited degradation, it leads to a minor change in impedance, often known as a "soft fault." As a soft fault gets worse, it may finally escalate into a hard fault, either an open circuit or a short circuit. Both types of faults can have severe costs, especially when wires play a vital role in the security of critical systems. As an example, studies conducted on the crashes of trans world airlines (TWA) Flight 800 in 1996 and Swiss Air Flight 111 in 1998 showed that the root cause was related to faulty wiring networks within the aircraft [1]. Safety is a critical factor in guaranteeing the optimal performance and functionality of these complicated systems. Reflectometry, a widely recognized technique for assessing the performance of wired networks, is commonly employed [1]. Time domain reflectometry (TDR) is a procedure that involves sending a specific signal into a complex electrical network at an injection point and subsequently analysing the signal's reflections. This process provides crucial information about the state of the electrical wiring network under test, allowing us to identify whether it is affected by faults or not. The diagnosis of wiring networks has been achieved using a variety of reflectometry techniques, including TDR, spectrum TDR (STDR), time frequency domain reflectometry (TFDR), and multicarrier TDR (MCTDR) [2–4]. The TDR methods alone cannot provide complete information about a complex wiring network. For detecting and locating faults, authors in [5, 6] compare the reflected signal of a healthy network with the reflected signal of a faulty network. As electrical networks increase in complexity, analysing the reflected signal in reflectometry can pose challenges. Consequently, many intelligent techniques have been combined with TDR to efficiently localize and identify faults. In this domain, numerous solutions have been proposed and can be broadly categorized into two types. The initial category includes methods that utilize the forward model in iterative optimization techniques to decrease the discrepancy between the measured response and the simulated response. This is achieved by employing optimization algorithms such as iterative-based optimization methods like genetic algorithm (GA) [7, 8], Electromagnetism-like mechanism (EM) [9], particle swarm optimization (PSO) [8, 10], teaching–learning-based optimization (TLBO) [11], backtracking search algorithm (BSA) [12], and black hole (BH) [13]. However, these methods suffer from a significant computation burden, that is, it takes a considerable amount of time for it to converge. The second category involves creating an adjusted model offline, incorporating data on the wiring network stored in a database. This model is then used online to facilitate fault detection and localization processes. The second type is more frequently exploited for complex wiring networks. In [14], the authors suggested using artificial neural networks (ANNs) for the inversion process, falling under the second category of techniques used in conjunction with TDR. However, as the responses of the wiring network can be conceptualized as high-dimensional data, employing this technique requires the development of a complex ANN with numerous internal parameters that necessitate regulation. To address this challenge, the authors in [15, 16] utilized the adaptive neuro-fuzzy inference system (ANFIS) as a solution. Support vector machine (SVM) has been employed in previous studies for diagnosing faults in power transmission lines [17–19], especially in cases where the wiring structure is straightforward with no complex branching. In a separate investigation [20], researchers addressed the challenge of branched wiring in their approach by utilizing the state transition matrix as the direct model for training the SVM. However, their proposed methodology had certain limitations. One of these limitations was associated with the forward model, which could only provide network's response at the injection point without capturing the impedance variations along the branches. This constraint might impede the generalization of the approach to other types of faults. Another limitation was the lack of fault characterization capability. Furthermore, in another study [21], SVM was effectively combined with principal component analysis (PCA) to identify faults in the wiring using TDR response. However, the proposed approach still faces challenges in terms of fault location accuracy, particularly when applied to complex networks. It proves to be particularly efficient in diagnosing straightforward yet intricate networks, especially those with three branches. In [22], the authors combined TDR with wavelet analysis and neural networks to locate faults in exceptionally long cables. In a previous investigation [23], the authors introduced a new method for detecting soft faults in wiring networks, combining reflectometry with principal component analysis. Moreover, in a related study [24], the authors presented an advanced technique for diagnosing soft faults in complex aircraft wiring networks, accommodating both noisy and noise-free scenarios. This method integrates reflectometry, subtractive correlation, and neural networks, significantly improving diagnostic accuracy.

This paper introduces an innovative wire network diagnosis method designed to effectively localize faults in complex wire networks. The proposed method comprises two main components. Firstly, a direct model based on the finite difference time domain (FDTD) method is established to emulate the TDR of the affected wire network. This step generates an offline dataset necessary for training the proposed model, which combines least-square SVM (LSSVM) and particle swarm optimization (PSO), referred to as PSO-LSSVM. In the second step, the PSO-LSSVM model is employed in real-time to accurately pinpoint the locations of faults in the measured reflectometry response.

This novel approach leverages the PSO algorithm in conjunction with the LSSVM method to achieve improved fault localization results. When compared to the existing literature, the proposed methodology proves to be well-suited for enhancing real-time diagnosis in complex wiring networks, emphasizing simplicity, speed, and accuracy as its distinguishing features.

To offer a comprehensive understanding of the methodology, the remainder of this paper is organized as follows. Section 2 elaborates on the construction of the forward model using the FDTD method. In Section 3, detailed information about the PSO-LSSVM technique is presented. Section 4 showcases the validation of the developed forward model, comparing it against measured data. The inversion results are demonstrated and discussed in Section 5. Finally, Section 6 concludes the

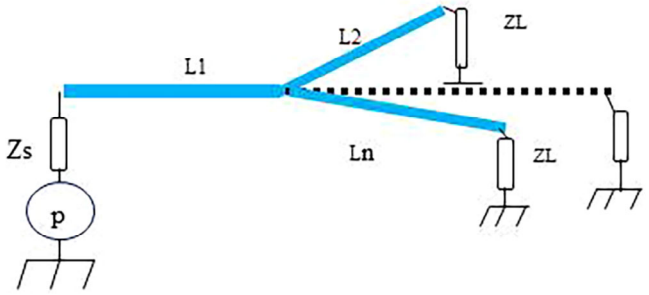

FIGURE 1 Healthy network.

study, summarizing the key findings and contributions of this research.

2 | THE FORWARD MODEL

A resistance, inductance, capacitance and conductance (RLCG) circuit model is employed to characterize the propagation in multiconductor transmission lines (MTLs) [25]:

$$\frac{\partial}{\partial z}u\left(z,t\right) = -R.i\left(z,t\right) - L.\frac{\partial}{\partial \mathrm{t}}i\left(z,t\right) \tag{1}$$

$$\frac{\partial}{\partial z}i\left(z,t\right) = -Gu\left(z,t\right) - C.\frac{\partial}{\partial t}u\left(z,t\right) \tag{2}$$

R, *L*, *C*, and *G* represent the series resistance, series inductance, shunt capacitance, and shunt conductance per unit length, respectively. Here, "*i*" and "*u*" denote the vectors of line currents and line voltages, respectively. Moreover, "*z*" and "*t*" symbolize the spatial and time variables. The time domain analysis of MTL is conducted through FDTD methods, wherein differential equations are converted into recursive finite difference equations. A finite difference method is used to approximate the derivatives in MTL equations. The sampling interval Δt and spatial cell size can be determined by checking the stability condition $\Delta t = \Delta z/v$. A wave propagates through transmission lines at a constant velocity or speed called *v*. For the case of a complex electrical network (as illustrated in Figure 1), the equations at the ends of each line (for z = 0 and z = l, respectively) are defined as follows:

Applying Equations (1) and (2), the FDTD method yields Equations (3) and (4) after a few calculations:

$$\left(\frac{[C]}{\Delta t} + \frac{[G]}{2}\right)\left([u\,(0)]^{n}\right) - \frac{[i\,(0)]^{n}}{\Delta z} = \left(\frac{[C]}{\Delta t} - \frac{[G]}{2}\right)$$

$$[u\,(0)]^{n-1} - \frac{[i_1^{n-1/2}]}{\Delta z/2} + \frac{[i\,(0)]^{n-1}}{\Delta z} \tag{3}$$

$$\left(\frac{[C]}{\Delta t} + \frac{[G]}{2}\right)[u\,(\ell)]^{n} + \frac{[i\,(\ell)]^{n}}{\Delta z} = \left(\frac{[C]}{\Delta t} - \frac{[G]}{2}\right)$$

$$[u\,(\ell)]^{n-1} + \frac{[i_{kmax}^{n-1/2}]}{\Delta z/2} - \frac{[i\,(\ell)]^{n-1}}{\Delta z} \tag{4}$$

Equation (3) specifies the voltages and currents at the line's source end (located at z = 0), while Equation (4) specifies the voltages and currents at the line's load end (located at z = ℓ). Based on Equations (3) and (4), we define the matrix Equation (5) for the entire network:

$$\mathrm{f}\left([\mathrm{x}]\right) = [\mathrm{A}]\,[\mathrm{X}] - [\mathrm{B}] = [0] \tag{5}$$

Each multiconductor line of index "*i*" is represented by voltages and currents at both ends, and the vector [X] contains the unknown currents and voltages at all network nodes. Within this context, there are two ends of a line indicated as 0 and ℓ at time t = $n\Delta t$. The variables, $u_i^n(0)$ and $i_i^n(0)$ correspond to the first end, while $u_i^n()$ and $i_i^n()$ pertain to the second end. By considering these factors, it is possible to define the X vector for a given line index i using Equation (6) as follows:

$$[\mathrm{X}] = \left[\ldots\left[u_k(0)^{\mathrm{n}}\right]\left[i_k(0)^{n}\right]\left[u_k(\ell)^{n}\right]\left[i_k(\ell)^{n}\right]\ldots.\right]^{\mathrm{T}} \tag{6}$$

In the network, unspecified currents and voltages are present at all nodes. The vector [X] comprises the voltages and currents at both ends of each multiconductor line with an assigned index *i*. The sub-matrices [A1] and [A2] constitute the matrix [A], with [A1 derived from the terminal conditions of the transmission line and specified by Equation (7):

$$[\mathrm{A1}] = \begin{bmatrix} [\mathrm{AL1}] & [0] & \ldots \\ [0] & [\mathrm{AL2}] & \ldots \\ \vdots & \vdots & \ddots \end{bmatrix} \tag{7}$$

[AL] is defined by Equation (8) for each branch *L* as:

$$[\mathrm{AL}] = \begin{bmatrix} \left(\frac{[c]}{\Delta t} + \frac{[G]}{2}\right) - \frac{1}{\Delta z}\left[1_{Ni}\right] & [0]\ [0] \\ [0]\ [0] & \left(\frac{[c]}{\Delta t} + \frac{[G]}{2}\right) + \frac{1}{\Delta z}\left[1_{Ni}\right] \end{bmatrix} \tag{8}$$

Ni: Takes a value of 1 for the case of lines with a single conductor or a matrix with diagonal containing 1 for multiline.

The sub-matrix [A2] is derived from the application of Kirchhoff's laws (KCL and KVL) to the endpoints and interconnections of the network using Equation (9).

$$\sum_{k=1}^{n}\left(\left[Y_k^m\right]\left[v_k^m\right] + \left[Z_k^m\right]\left[i_k^m\right]\right) = \left[P^m\right] \tag{9}$$

The principles of Kirchhoff's laws, namely Kirchhoff's current law (KCL) and Kirchhoff's voltage law (KVL), are applied at the junctions of the network, including extremities and interconnections. Additionally, these laws are used to analyse the impedances or admittances of the network's node with index m, leading to the formation of matrices $[Z_k^m]$ and $[Y_k^m]$.

$[P^m]$: Represent the vector of localized sources of current or voltage.

An equivalent source is represented by [B] as illustrated using Equation (10), which consists of two sub-vectors [B1] and [B2],

where:

$$[\mathrm{B1}] = \begin{bmatrix} [\mathrm{BL1}] \\ [\mathrm{BL2}] \\ \vdots \end{bmatrix} \tag{10}$$

For each line, [BL] contains the second term of Equations (3) and (4) and defined by Equation (11):

$$[\mathrm{BL}] = \begin{bmatrix} \left(\frac{[C]}{\Delta t} - \frac{[G]}{2}\right)[u(0)]^{n-1} - \frac{[i_1^{n-1/2}]}{\Delta z/2} + \frac{[i(0)]^{n-1}}{\Delta z} \\ \left(\frac{[C]}{\Delta t} - \frac{[G]}{2}\right)[u(\ell)]^{n-1} + \frac{[i_{kmax}^{n-1/2}]}{\Delta z/2} - \frac{[i(\ell)]^{n-1}}{\Delta z} \end{bmatrix} \tag{11}$$

[B2] is represented by Equation (12):

$$[\mathrm{B2}] = \begin{bmatrix} \vdots \\ [P^m] \\ \vdots \end{bmatrix} \tag{12}$$

At every time step, the solution of matrix Equation (5) gives the currents and voltages in every node of the network. Recurrence Equations (13) and (14) are then used to give the currents and voltages in each space increment.

$$[u_k^n] = \left([C]\frac{\Delta z}{\Delta t} + [G]\frac{\Delta z}{2}\right)^{-1}\left[\left([C]\frac{\Delta z}{\Delta t} - [G]\frac{\Delta z}{2}\right)[u_k^{n-1}] - \left([i_k^{n-1/2}] - [i_{k-1}^{n-1/2}]\right)\right] \quad K = 2, 3, \ldots\ldots\ldots\ldots k_{\max} \tag{13}$$

$$\left[i_k^{n+1/2}\right] = \left([L]\frac{\Delta z}{\Delta t} + [R]\frac{\Delta z}{2}\right)^{-1}\left[\left([L]\frac{\Delta z}{\Delta t} - [R]\frac{\Delta z}{2}\right)\left(\left[i_k^{n-1/2}\right]\right) - \left([u_{k+1}^n] - [u_k^n]\right)\right] \quad K = 1, 2, \ldots\ldots\ldots\ldots k_{\max} \tag{14}$$

Where: $k_{\max}$ yield the number max of line space step Δz.

A soft fault has been modelled as a transmission line with parameters per unit-length R_{def}, C_{def}, L_{def}, G_{def}, as presented in Figure 2. Taking all tube terminal conditions into account, the submatrix [A1] is defined by (15)

$$[\mathrm{A1}] = \begin{bmatrix} [\mathrm{AL1}] & \cdots & [0] & \ldots \\ \vdots & \ddots & \vdots & \\ [0] & \ldots & [\mathrm{AL_{def}}] & \ldots \\ [0] & & [0] & \ldots \end{bmatrix} \tag{15}$$

where $[\mathrm{AL_{def}}]$ represents [AL] of soft fault and is given by Equation (16):

$$[\mathrm{AL_{def}}] = \begin{bmatrix} \left(\frac{[C_{\mathrm{def}}]}{\Delta t} + \frac{[G_{\mathrm{def}}]}{2}\right) - \frac{1}{\Delta z}[1_{Ni}] & [0]\ [0] \\ [0]\ [0] & \left(\frac{[C_{\mathrm{def}}]}{\Delta t} + \frac{[G_{\mathrm{def}}]}{2}\right) + \frac{1}{\Delta z}[1_{Ni}] \end{bmatrix} \tag{16}$$

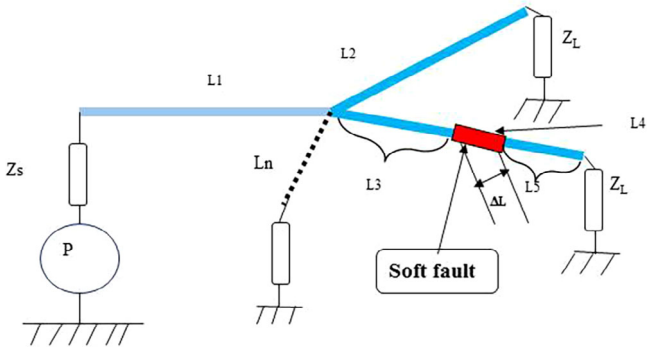

FIGURE 2 Faulty network.

While [B1] is defined by Equation (17):

$$[\mathrm{B1}] = \begin{bmatrix} [\mathrm{BL1}] \\ \vdots \\ [\mathrm{BL_{def}}] \\ \vdots \\ \vdots \end{bmatrix} \tag{17}$$

where $[\mathrm{BL_{def}}]$ is represented by Equation (18):

$$[\mathrm{BL_{def}}] = \begin{bmatrix} \left(\frac{[C_{\mathrm{def}}]}{\Delta t} - \frac{[G_{\mathrm{def}}]}{2}\right)[u(0)]^{n-1} - \frac{[i_1^{n-1/2}]}{\Delta z/2} + \frac{[i(0)]^{n-1}}{\Delta z} \\ \left(\frac{[C_{\mathrm{def}}]}{\Delta t} - \frac{[G_{\mathrm{def}}]}{2}\right)[u(\ell)]^{n-1} + \frac{[i_{kmax}^{n-1/2}]}{\Delta z/2} - \frac{[i(\ell)]^{n-1}}{\Delta z} \end{bmatrix} \tag{18}$$

In order to calculate the spaced current and voltage distribution of the soft fault, the so-called recurrence of (19) and (20) has been used.

$$[u_k^n] = \left([C_{\mathrm{def}}]\frac{\Delta z}{\Delta t} + [G_{\mathrm{def}}]\frac{\Delta z}{2}\right)^{-1}\left[\left([C_{\mathrm{def}}]\frac{\Delta z}{\Delta t} - [G_{\mathrm{def}}]\frac{\Delta z}{2}\right)[u_k^{n-1}] - \left([i_k^{n-1/2}] - [i_{k-1}^{n-1/2}]\right)\right] \quad K = 2, 3, \ldots\ldots\ldots\ldots k_{\max} \tag{19}$$

$$\left[i_k^{n+1/2}\right] = \left([L_{\mathrm{def}}]\frac{\Delta z}{\Delta t} + [R_{\mathrm{def}}]\frac{\Delta z}{2}\right)^{-1}\left[\left([L_{\mathrm{def}}]\frac{\Delta z}{\Delta t} - [R_{\mathrm{def}}]\frac{\Delta z}{2}\right)\left[i_k^{n-1/2}\right] - \left([u_{k+1}^n] - [u_k^n]\right)\right] \quad K = 1, 2, \ldots\ldots\ldots\ldots k_{\max} \tag{20}$$

3 | PSO-LSSVM FOR FUNCTION ESTIMATION

Support vector machine (SVM) is a powerful and widely used supervised machine learning algorithm used for classification and regression tasks. It is based on statistical learning theory; Vapnik introduced SVM [26], a relatively new and effective machine learning method. Solving the non-linear equations required for an SVM model can be challenging. LSSVM, on the other hand, formulates the SVM as a regularized least squares regression problem Unlike directly optimizing for the margin, LSSVM minimizes the error between predicted outputs and target outputs using a squared loss function, as proposed by Suykens et al [27]. LSSVM is defined as follows.

Assume a training set $(x_k, y_k)_{k=1}^{N}$ with input data $x_k \in R^n$ and output data $y_k \in R$, the LSSVM model for function approximation has the following representation using Equation (21) in the feature space:

$$y(x) = w^T \varphi(x) + b \tag{21}$$

Here the non-linear function $\varphi(.)$: $R^n \rightarrow R^n k$ maps the input space to a higher dimension feature space. b is a bias term and $w \in R^n$ is a weight vector. The optimization problem is defined using Equation (22) as:

$$\min J(w, e) = \frac{1}{2} w^T w + \gamma \frac{1}{2} \sum_{i=1}^{N} e_i^2 \tag{22}$$

Subject to the equality constraints illustrated in Equation (23):

$$y_i = w^T \varphi(x_i) + b + e_i \quad i = 1, \ldots, N \tag{23}$$

In this case, e_i represents the fitting error. The smoothness of the function y and fitting precision are traded off according to the hyper-parameter γ . It is possible to create a Lagrangian equation illustrated in (24):

$$L(w, b, \xi, \alpha) = J(w, b, \xi) - \sum_{i=1}^{N} \alpha_i \{w^T \cdot \varphi(x_i) + b - y_i + \xi_i\} \tag{24}$$

In this case, a_i and R are called a support vector and represents the Lagrange multiplier. The following equations must be satisfied based on the optimization conditions illustrated in Equation (25):

$$\begin{cases} \frac{\partial L}{\partial w} = 0 \rightarrow w = \sum_{i=1}^{N} \alpha_i \varphi(x_i) \\ \frac{\partial L}{\partial b} = 0 \rightarrow \sum_{i=1}^{N} \alpha_i = 0 \\ \frac{\partial L}{\partial e_i} = 0 \rightarrow \alpha_i = \gamma e_i \; i = 1, \ldots, N \\ \frac{\partial L}{\partial \alpha_i} = 0 \rightarrow y_i = w^T \varphi(x_i) + b + e_i \; i = 1, \ldots, N \end{cases} \tag{25}$$

Eliminating w and e will result in a linear system instead of a quadratic programming issue as illustrated in Equation (26).

$$\begin{bmatrix} 0 & I_N^T \\ I_N & \Omega + \gamma^{-1} \cdot I_N \end{bmatrix} \begin{bmatrix} b \\ \alpha \end{bmatrix} = \begin{bmatrix} 0 \\ Y \end{bmatrix} \tag{26}$$

where

$$Y = [y_1, \ldots, y_N]^T, \; I_N = [1, \ldots, 1]^T, \alpha = [\alpha_1, \ldots, \alpha_N]^T$$

In accordance with the Mercer conditions [26], SVM maintains its choice of kernel function $K(.,.)$ from a range of linear, polynomial, radial basis, and multilayer perceptron functions. In LSSVM as well as this work, the RBF kernel is illustrated in Equation (27) often used.

$$K(x, x_k) = \exp\left(-\frac{x - x_k}{\sigma^2}\right) \tag{27}$$

where σ is kernel width.

The final LSSVM model for function estimation is transformed into Equation (28):

$$y(x) = \sum_{i=1}^{N} \alpha_i K(x, x_i) + b N \tag{28}$$

where α_i and b are the solution to (26).

3.1 | LSSVM regularization

The idea of combining PSO with LSSVM is to use the PSO algorithm to search for the optimal parameters of the LSSVM model. The parameters to be optimized typically include the regularization parameter (γ and σ^2) and the kernel parameters (if a kernel function is used). An LSSVM's performance depends on its hyper-parameters which are with the radial basis function (RBF) kernel, γ and σ^2. There are several methods for finding these parameters, each with its own advantages and disadvantages. This paper utilizes an optimization technique known as particle swarm optimization.

3.2 | Particle swarm optimization

To optimize objective functions, the PSO method employs a population-based search [28]. In this metaphorical representation, particles are likened to birds in a flock, symbolizing various solutions to the given situation. These particles, generated randomly, move freely within the multidimensional search space. The particle search optimization technique aims to progressively approach the global optimal point by considering the best position obtained by an individual particle p_{best} and the best position acquired by the group g_{best}, both originating from various starting locations.

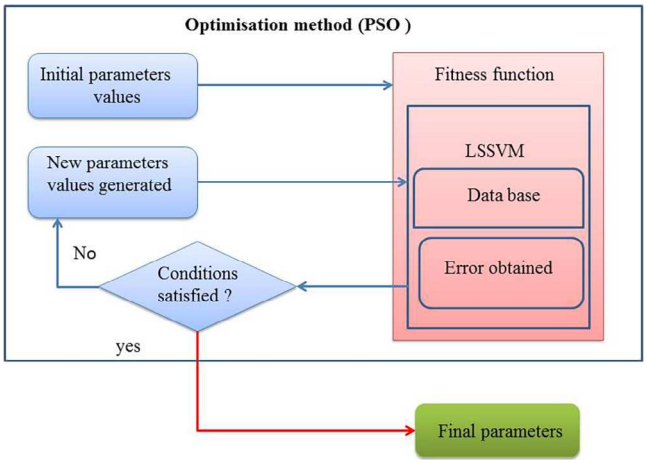

FIGURE 3 Particle swarm optimization (PSO)-based hyper-parameter selection process for least square support vector machine (LSSVM) parameter optimization.

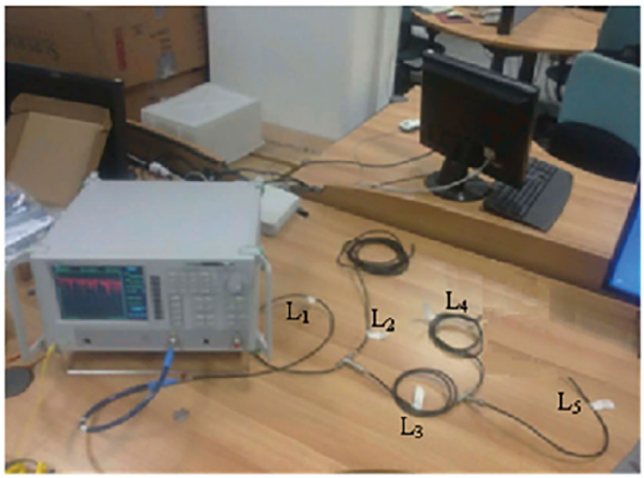

FIGURE 4 Experimental setup.

The LSSVM hyper parameters, γ and σ^2, are optimized by taking advantage of the various directions offered by the p_{best} and g_{best} particles. The Figure 3 depicts the proposed approach, which tackles the LSSVM parameter optimization problem by using an optimization-based hyper-parameter selection technique (Equations 29–30).

$$\min f\left(\gamma, \sigma^2\right) = \min(\text{RMSE}) \tag{29}$$

$$\text{subject to} \begin{cases} \gamma_{\text{lower}} \leqslant \gamma \leqslant \gamma_{\text{upper}} \\ \sigma^2_{\text{lower}} \leqslant \sigma^2 \leqslant \sigma^2_{\text{upper}} \end{cases} \tag{30}$$

With the root mean square error (RMSE) defined using Equation (31):

$$\text{RMSE} = \sqrt{\frac{1}{N}\sum_{i=1}^{N}\left(\frac{y_i - \hat{y}\left(\gamma, \sigma^2\right)}{y_i}\right)^2} \times 100\% \tag{31}$$

Here, the value of the fault parameter is denoted by y_i, while the LSSVM produces a predicted value denoted by $\widehat{y_i}$. The validation data set contains N samples.

4 | VALIDATION OF THE DEVELOPED FORWARD MODEL

As mentioned earlier, TDR serves as a valuable technique for measuring impedance values alongside the line and identifying disturbances in distance or time. The fundamental approach for TDR measurements involves injecting a signal into the coaxial cable's inner conductor. As the signal travels along the cable, encountering a disruption causes a portion of its energy to reflect back to the injection point, where it is subsequently collected. In this study, TDR responses were measured using an experimental setup that employed a vector network analyser (VNA), as illustrated in Figure 4. The network under test (NUT) is connected to the testing port of the VNA using a suitable connector wire (the blue wire with a length of 50 cm) to carry out the measurements. For accurate results, it is important to calibrate the VNA before performing any measurements. This calibration compensates for the presence of the connector cable between the measuring port (on the VNA side) and the desired testing port on the NUT side.

The VNA measures the NUT response in the frequency domain, represented by the S11 parameter. This frequency-domain response is mathematically converted into the time domain using an inverse fast fourier transform (IFFT) [29].

4.1 | Case of Y shaped network

A Y-shaped network is employed to test the forward model using measured data. The RG58 CU coaxial cable utilized in this network is illustrated in Figure 5. The determined and computed values of the distributed parameters (L, C, R, and G) are provided below in accordance with [30]. The radii of the inner, outer, and external conductors are represented by the values of A, R_i, and R_0, respectively. The terms μ and ε, respectively, describe the material's dielectric permittivity and magnetic permeability, between the conductors. Additionally, $tg(\delta)$ stands for the tangent of the dielectric loss. To assess the performance of the proposed model, a raised cosine pulse was used as a source signal. The raised cosine pulse with a rising time of 4 ns and amplitude of 1 V is employed as input for the FDTD algorithm, as shown in (32):

$$e(t) = \begin{cases} 0.5\left(1 - \cos\left(2\pi F t\right)\right) & 0 < t < \frac{1}{F} \\ 0 & \text{otherwise} \end{cases} \tag{32}$$

The Figure 6 shows a schematic of the Y-shaped network that was adopted in this case. Three branches make up this network: $L_1 = 1$ m, $L_2 = 4$ m, and $L_3 = 1$ m. The type of load at the end of each branch is an open circuit, as illustrated.

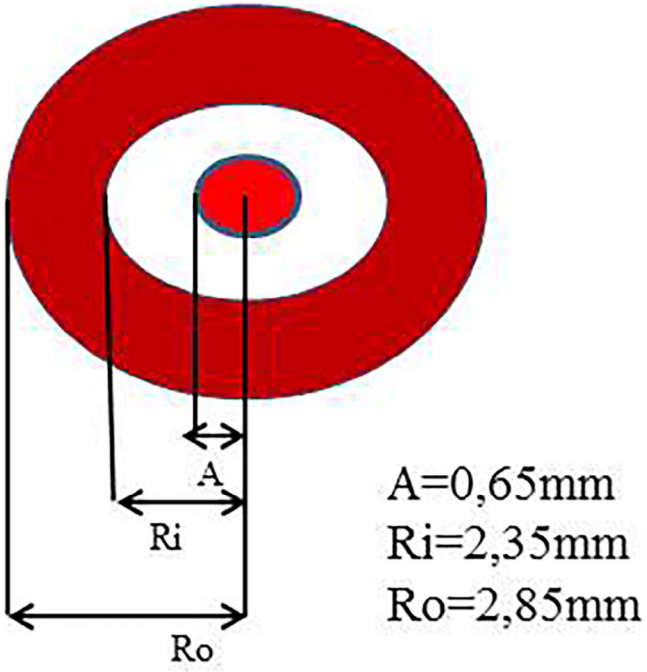

FIGURE 5 The used cable cross section of.

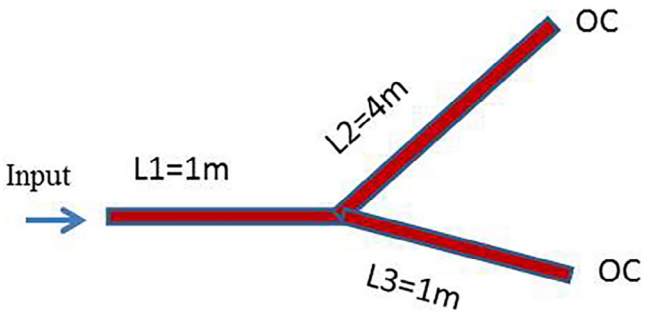

FIGURE 6 The Y-shaped network utilized to verify the forward model.

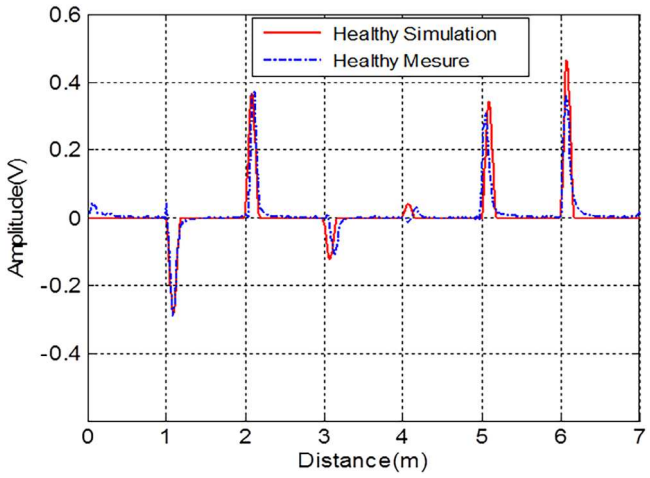

FIGURE 7 Measuring and simulating the TDR responses of the healthy Y-shaped network.

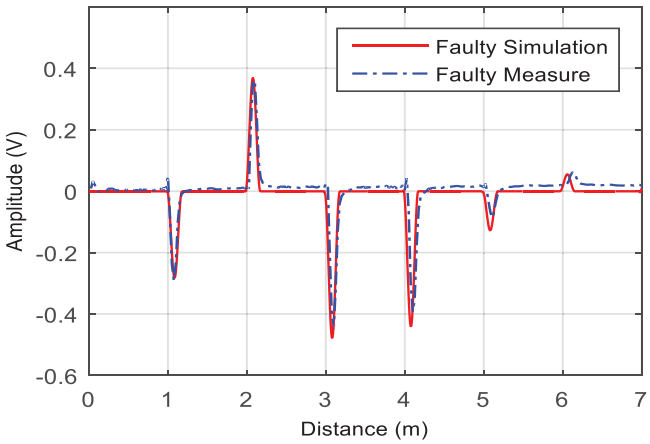

FIGURE 8 Measuring and simulating the TDR responses of the faulty Y-shaped network.

A comparison of the TDR response of a healthy wire network produced by the provided forward model and the response established through measurement is shown in Figure 7. The figure clearly illustrates how closely the measured and simulated TDR responses correspond. Variations in the cable's ideal and actual characteristic impedance may cause slight differences between the measured and simulated responses.

Another scenario involving a Y-shaped network with a hard fault (short circuit) occurring in the second branch (L_2), is investigated in this paper. The fault is precisely 3 m away from the input position. The measured and modelled TDR responses for this specific situation are contrasted in Figure 8. The remarkable resemblance between the measured and generated TDR responses is clearly shown in the figure.

4.2 | Case of YY shaped network

The study also addresses a faulty YY-shaped wire network, as seen in Figure 9. The network comprises five branches

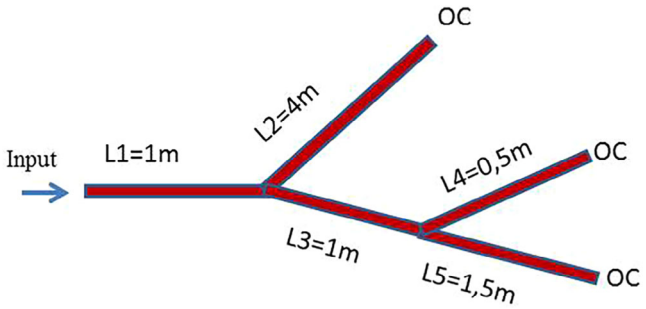

FIGURE 9 The YY-shaped network utilized to verify the forward model.

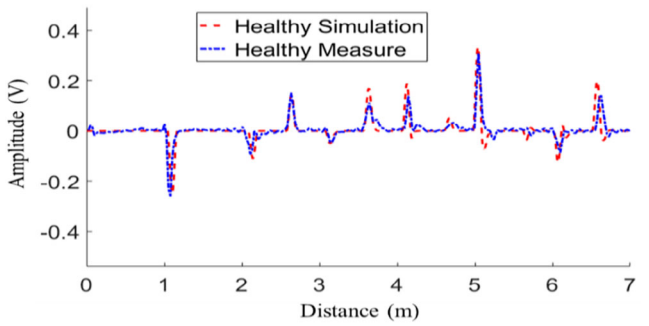

FIGURE 10 YY-shaped network TDR measured and simulated responses.

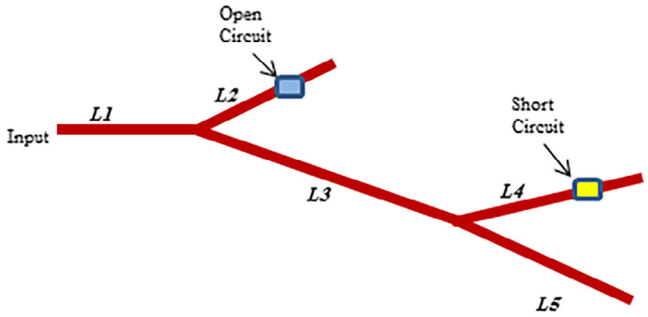

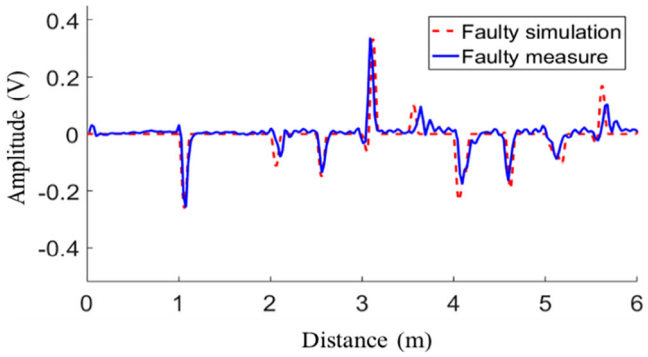

FIGURE 11 Faulty YY-shaped network TDR measured and simulated responses.

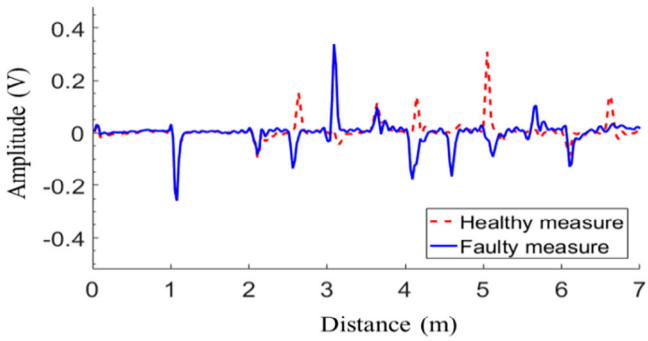

FIGURE 12 Comparison between the measured TDR responses of the healthy and the faulty YY-shaped networks.

with lengths as follows: $L_1 = 1$ m, $L_2 = 4$ m, $L_3 = 1$ m, $L_4 = 0.5$ m, and $L_5 = 1.5$ m. The type of load at the end of each branch is an open circuit, as illustrated in Figure 9. Branch L_4 experiences a short circuit 0.4 m from the second junction, while branch L_2 is affected by an open circuit fault occurring 2 m from the first junction. The measured and modelled TDR responses for the YY-shaped network are shown in Figure 10. Figure 11 on the other hand, displays the simulated and measured TDR responses for the faulty YY-shaped network. Figure 12 shows the TDR measurement results for both the healthy and faulty YY-shaped networks. The small variation between the results obtained from measurements and simulations is attributed to differences between a cable's theoretical characteristic impedance and its practical impedance.

5 | INVERSION RESULTS

5.1 | Case of the Y-shaped network configuration

The new method, called PSO-LSSVM, is employed to analyse the faulty Y-shaped network presented earlier. With this method, the inverse problem is solved by leveraging the voltage signal differences between the healthy and damaged networks. The maximum value and the corresponding appearance time (t) are obtained by calculating this difference. The use of this time parameter facilitates the localization of the fault. The Figure 13 provides an overview of the suggested approach's technique and a clear graphic representation of it.

TABLE 1 Parameters of the PSO-LSSVM model with RBF kernel (case of Y shaped network).

	Training	Validation	Test	γ	$\sigma 2$	RMSE%
Particle swarm optimization - least square support vector machine (PSO-LSSVM)	1000	400	460	2.2758×10^9	51.7947	0.034

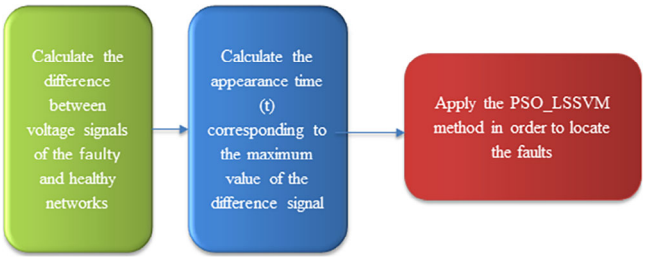

FIGURE 13 Diagram of proposed approach based on particle swam optimization - least square support vector machine (PSO-LSSVM).

TABLE 2 . Estimated and obtained values of fault locations case of Y shaped network.

Actual fault position	Estimated fault using particle swarm optimization - least square support vector machine (PSO-LSSVM)	The relative error
0.7920	0.7941	2.65×10^{-3}
1.8672	1.8668	0.21×10^{-3}
2.0952	2.0948	0.19×10^{-3}
3.5760	3.5758	0.05×10^{-3}
4.8096	4.8100	0.08×10^{-3}

The training database for the PSO-**LS**SVM model is created using the forward model, which is based on the FDTD approach. Input data, specifically the appearance time (t), and related output data, indicating the fault location, are both included in this database. A total of 1860 random and normalized samples were generated across three sets of data for training and testing the PSO-LSSVM model. The first 1000 samples of these were used for model training, the next 400 samples for parameter validation, and the remaining 460 examples for model testing. With the RBF kernel chosen, the PSO-LSSVM technique was employed to complete the inversion process. The estimated real value of the fault location was represented using a single-output PSO-**LS**SVM model. In this study, the performance of the PSO-LSSVM model was assessed using the root mean square error (RMSE) as the performance parameter. The parameters of the PSO-LSSVM model with the RBF kernel are summarized in Table 1.

The fault given by the PSO-LSSVM model and the fault present in the testing database are compared in Figure 14. The PSO-LSSVM model can effectively estimate the values of faults, as illustrated by these results, demonstrating its generalization capability. Table 2 represents some estimated and

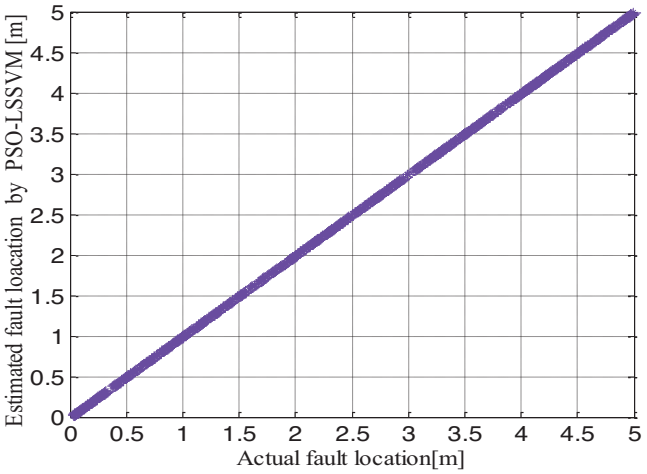

FIGURE 14 Comparison between the faults locations estimated by the particle swarm optimization - least square support vector machine (PSO-LSSVM) and the faults included in the testing data sets.

obtained values of faults in the case of the Y-shaped network. The results displayed in Table 2 improve the efficiency of PSO-LSSVM in fault location for the case of Y-shaped network.

$$\text{Relative error} = \left| \frac{\text{Approximate value} - \text{Exact value}}{\text{Exact value}} \right|$$

5.2 | Case of the YY-shaped network configuration

The YY-shaped network, depicted in Figure 9, is observed as a more complicated network in this research than the initial one. $L_1 = 1$ m, $L_2 = 4$ m, $L_3 = 1$ m, $L_4 = 0.5$ m, and $L_5 = 1.5$ m are the lengths of the network's branches. The forward model is used to produce the requisite database for training the PSO-LSSVM model. For training and testing the PSO-LSSVM model, three data sets were prepared, totalling 2080, random and normalized samples. The first 1000 data points were used for model training, the next 400 for parameter validation, and the last 680 for model testing. The PSO-LSSVM approach with the RBF kernel was used to perform the inversion. To represent the estimated real value of the fault location, a single-output PSO-LSSVM model was used. The RMSE was used as a performance factor to assess the accuracy of the PSO-LSSVM model. Figure 15 also shows a significant agreement between the estimated fault locations obtained using

TABLE 3 Parameters of the PSO-LSSVM model with RBF kernel case of YY shaped network.

	Training	Validation	Test	γ	$\sigma 2$	RMSE%
Particle swarm optimization - least square support vector machine (PSO-LSSVM)	1000	400	680	1.0000×10^{10}	7.1968×10^{4}	0.040

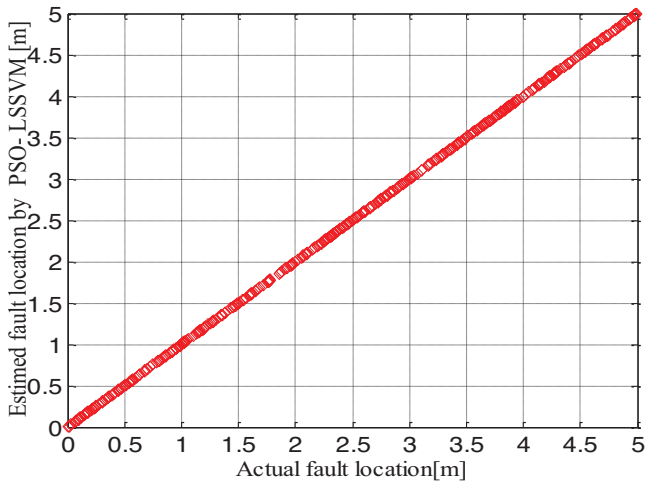

FIGURE 15 Comparison between the faults locations estimated by the particle swarm optimization - least square support vector machine (PSO-LSSVM) and the faults included in the testing data sets.

TABLE 4 Estimated and obtained values of fault locations case of YY shaped network.

Actual fault position	Estimated fault using PSO-LSSVM	The relative error
4.9320	4.9323	0.06×10^{-3}
3.6168	3.6167	0.02×10^{-3}
2.4480	2.4477	0.12×10^{-3}
1.7592	1.7589	0.17×10^{-3}
0.5760	0.5758	0.34×10^{-3}

PSO-LSSVM and those in the database. Table 3 shows the parameters of the PSO-LSSVM model using the RBF kernel.

The PSO-LSSVM model can effectively estimate the values of faults, as illustrated by these results, which demonstrate its generalization capability. Table 4 represents some estimated and obtained values of faults in the case of the YY-shaped network. The results displayed in Table 4 further improve the efficiency of PSO-LSSVM in fault location for the YY-shaped network.

5.3 | Comparison with the existing literature

As stated in Table 5, the proposed algorithm has been compared with other algorithm results in order to determine its

TABLE 5 Comparison with published work.

	Error	Computational time
Particle swarm optimization - least square support vector machine (PSO-LSSVM)	3.7×10^{-4} m	1 s
Support vector machine (SVM) [20]	1 cm	1s
Genetic algorithm (GA) [10]	7.48 cm	94.60 min
Particle swarm optimisation (PSO) [10]	4.68 cm	26.36 min
Electromagnetism-like mechanism (EM) [9]	6.5 cm	–
Improved black hole (IBH) algorithm [13]	1.93 cm	20.00 min

effectiveness and accuracy. We list the errors in the lengths of the impacted branches in this table along with the total amount of computation time and inaccuracy. The suggested approach is extremely effective and faster than those realized in the literature, as shown by Table 5. LSSVM typically outperforms SVM quadratic programming in terms of speed, as it involves solving a linear system of equations, while SVM quadratic programming tackles a more complex quadratic programming problem. Our proposed approach leverages PSO in a two-phase optimization for training the LSSVM model, offering distinct advantages. Firstly, by employing PSO for training, our method effectively optimizes the hyper parameters of the LSSVM model, leading to enhanced prediction accuracy. Secondly, the inherent computational efficiency of the LSSVM model, attributable to its linear system of equations, contributes to an overall expedited training process. The training time for the PSO-LSSVM is approximately 15 min for the Y-shaped network and around 16 min for the YY network. The PSO-LSSVM training can be conducted offline. The inversion process using this method is exceptionally rapid, taking less than 1 s, with minimal error, making it suitable for online applications. The cumulative error using PSO-LSSVM is 3.7×10^{-4} m, which is significantly less than the errors observed in IBH (1.93 cm), PSO (4.68 cm), EM (6.5 cm), and GA (7.48 cm), respectively. Even the SVM mentioned in [21] exhibited a runtime of less than 1 s, but with an error of more than 1 cm.

6 | CONCLUSION

In conclusion, this research introduces a novel and effective methodology for diagnosing complex wire networks by

employing TDR in combination with the PSO and least squares support vector machine LSSVM algorithm. The establishment of a forward model using RLCG parameters and the FDTD method permits the modelling of the TDR response for a specific complex wire network. The application of the PSO-LSSVM approach effectively addresses the inverse problem, allowing for the localization of faults within these networks. The experimental results validate the practicality and effectiveness of this integrated approach in real-world systems. Clearly, the proposed technique, combining TDR and PSO-LSSVM, emerges as a robust and reliable diagnostic tool for complex wire networks, offering promising implications for fault localization in practical applications. The results prove that the proposed methodology outperforms various iterative methods in the literature, including GA, PSO, IBH, and EM. Furthermore, this research has the potential to be expanded to address soft faults, thereby improving the accuracy and reliability of wire network diagnosis.

AUTHOR CONTRIBUTIONS

Abderrzak Laib: Conceptualization; methodology; software; formal analysis; investigation; writing—original draft. **Mohamed Chelabi**: Conceptualization; methodology; software; formal analysis; investigation; writing—original draft; writing—review & editing. **Yacine Terriche**: Conceptualization; supervision; writing—review & editing. **Mohammed Melit**: Conceptualization; supervision; writing—review & editing. **Hamza Boudjefdjouf**: Conceptualization; supervision; writing—review & editing. **Hafiz Ahmed**: Conceptualization; supervision; project management; writing—review and editing. **Zakaria Chedjara**: Conceptualization; supervision; writing—review & editing.

CONFLICT OF INTEREST STATEMENT

The authors declare no conflict of interest.

DATA AVAILABILITY STATEMENT

Data sharing not applicable—no new data generated.

ORCID

Hafiz Ahmed https://orcid.org/0000-0001-8952-4190

REFERENCES

1. Furse, C., Chung, Y.C., Lo, C., Pendayala, P.: A critical comparison of reflectometry methods for location of wiring faults. Smart Struct. Syst. 2(1), 25–46 (2006)
2. Sharma, C.R., Furse, C., Harrison, R.R.: Low power STDR CMOS sensor for locating faults in aging aircraft wiring. IEEE Sens. J. 7(1), 43–50 (2007)
3. Furse, C., Smith, P., Safavi, M., Lo, C.: Feasibility of spread spectrum sensors for location of arcs on live wires. IEEE Sens. J. 5(6), 1445–1450 (2005)
4. Lelong, A., Carrion, M.O.: On line wire diagnosis using multicarrier time domain reflectometry for fault location. In: *SENSORS, 2009 IEEE*, pp. 751–754. IEEE, Piscataway, NJ (2009)
5. Griffiths, L.A., Parakh, R., Furse, C., Baker, B.: The invisible fray: A critical analysis of the use of reflectometry for fray location. IEEE Sens. J. 6(3), 697–706 (2006)
6. Furse, C., Smith, P., Diamond, M.: Feasibility of reflectometry for nondestructive evaluation of prestressed concrete anchors. IEEE Sens. J. 9(11), 1322–1329 (2009)
7. Smail, M.K., Pichon, L., Olivas, M., Auzanneau, F., Lambert, M.: Detection of defects in wiring networks using time domain reflectometry. IEEE Trans. Magn. 46(8), 2998–3001 (2010)
8. Smail, M.K., Bouchekara, H.R.E.H., Pichon, L., Boudjefdjouf, H., Mehasni, R.: Diagnosis of wiring networks using particle swarm optimization and genetic algorithms. Comput. Electr. Eng. 40(7), 2236–2245 (2014)
9. Bouchekara, H.R.E.H., Smail, M.K., Dahman, G.: Diagnosis of multi-fault wiring network using time-domain reflectometry and electromagnetism-like mechanism. Electromagnetics 33(2), 131–143 (2013)
10. Boudjefdjouf, H., Mehasni, R., Bouchekara, H.R.E.H., Orlandi, A., de Paulis, F.: Non-destructive testing in complexes cabling networks using time domain reflectometry and particle swarm optimization. Ann. Comput. Sci. Inf. Syst. 3, 157–163 (2014)
11. Boudjefdjouf, H., Mehasni, R., Orlandi, A., Bouchekara, H.R.E.H., de Paulis, F., Smail, M.K.: Diagnosis of multiple wiring faults using time-domain reflectometry and teaching–learning-based optimization. Electromagnetics 35(1), 10–24 (2015)
12. Boudjefdjouf, H., Bouchekara, H.R.E.H., de Paulis, F., Smail, M.K., Orlandi, A., Mehasni, R.: Wire fault diagnosis based on time-domain reflectometry and backtracking search optimization algorithm. ACES J. 31(4), 340–347 (2016)
13. Smail, M.K., Bouchekara, H.R.E.H., Pichon, L., Boudjefdjouf, H., Amloune, A., Lacheheb, Z.: Non-destructive diagnosis of wiring networks using time domain reflectometry and an improved black hole algorithm. Nondestruct. Test. Eval. 32(3), 286–300 (2017)
14. Smail, M.K., Hacib, T., Pichon, L., Loete, F.: Detection and location of defects in wiring networks using time-domain reflectometry and neural networks. IEEE Trans. Magn. 47(5), 1502–1505 (2011)
15. Laib, A., Melit, M., Nekhoul, B., Boudjefdjouf, H., Bouchekara, H.: Localisation of faults in wiring networks using time domain reflectometry and adaptive neuro-fuzzy inference system. Electron. Lett. 53(9), 600–602 (2017)
16. Laib, A., Melit, M., Nekhoul, B., Kerroum, K., Drissi, K.: Soft fault identification in electrical network using time domain reflectometry and adaptive neuro-fuzzy inference system. In: *2017 5th International Conference on Electrical Engineering—Boumerdes (ICEE-B)*, pp. 1–4. IEEE, Piscataway, NJ (2017)
17. Ravikumar, B., Thukaram, D., Khincha, H.P.: Application of support vector machines for fault diagnosis in power transmission system. IET Gener. Transm. Distrib. 2(1), 119–130 (2008)
18. Salat, R., Osowski, S.: Accurate fault location in the power transmission line using support vector machine approach. IEEE Trans. Power Syst. 19(2), 979–986 (2004)
19. Ray, P., Mishra, D.P.: Support vector machine based fault classification and location of a long transmission line. Eng. Sci. Technol. Int. J. 19(3), 1368–1380 (2016)
20. Zhang, X., Zhang, M., Liu, D.: Reconstruction of faulty cable network using time-domain reflectometry. Prog. Electromagn. Res. 136, 457–478 (2013)
21. Smail, M.K., Boubezoul, A., Bouchekara, H.R.E.H., Sellami, Y.: Wiring networks diagnosis using time-domain reflectometry and support vector machines. IET Sci. Meas. Technol. 14(2), 220–224 (2020)
22. Laib, A., Melit, M., Nekhoul, B., Kerroum, K., Drissi, K.E.: A new hybrid approach using time-domain reflectometry combined with wavelet and neural network for fault identification in wiring network. In: *Proceedings of the 2016 8th International Conference on Modelling, Identification and Control (ICMIC)*, pp. 290–295. IEEE, Piscataway, NJ (2016)
23. Taki, N., Delpha, C., Diallo, D., Ben Hassen, W., Ravot, N.: Soft fault diagnosis in wiring networks using reflectometry and principal component analysis. Measurement 198, 111378 (2022)
24. Laib, A., Terriche, Y., Melit, M., Su, C.-L., Mutarraf, M.U., Bouchekara, H.R.E.H., Guerrero, J.M., Boudjefdjouf, H.: Enhanced artificial intelligence technique for soft fault localization and identification in complex aircraft microgrids. Eng. Appl. Artif. Intell. 127, 107289 (2024)
25. Paul, C.: Analysis of Multiconductor Transmission Lines. Wiley, New York (1994)

26. Valyon, J., Horvath, G.: A robust LS-SVM regression. World Acad. Sci., Eng. Technol. 7, 148–153 (2005)
27. Vapnik, V.N.: Statistical Learning Theory. Wiley, New York (1998)
28. Nabavi-Kerizi, S.H., Abadi, M., Kabir, E.: A PSO based weighting method for linear combination of neural networks. Comput. Electr. Eng. 36(5), 886–894 (2010)
29. De Paulis, F., Boudjefdjouf, H., Bouchekara, H.R.E.H., Orlandi, A., Smail, M.K.: Performance improvements of wire fault diagnosis approach based on time-domain reflectometry. IET Sci. Meas. Technol. 11(5), 538–544 (2017)
30. Halliday, D., Resnick, R.: Physics, vol. 2, 2nd ed., John Wiley & Sons, New York (1962)

How to cite this article: Laib, A., Chelabi, M., Terriche, Y., Melit, M., Boudjefdjouf, H., Ahmed, H., Chedjara, Z.: Enhanced complex wire fault diagnosis via integration of time domain reflectometry and particle swarm optimization with least square support vector machine. IET Sci. Meas. Technol. 1–12 (2024). https://doi.org/10.1049/smt2.12187